Development of Standardized Property Requirements, Measurement Methods, and Reporting Guidance for Coatings

Nuclear Technology Research and Development

Approved for public release.
Distribution is unlimited.

Prepared for
U.S. Department of Energy
Tim Graening
Peter Mouche
Ryan Sweet
Padhraic L. Mulligan
Kory Linton
Andrew Nelson
Oak Ridge National Laboratory

01/15/2021
M4FT-21OR020202013
ORNL/SPR-2021/6

SUMMARY

The diverse research programs presently in progress around the world have advanced a large number of coated cladding concepts to various stages of maturity. Industry teams have developed leading coating compositions and geometries, but significant disparity exists in the importance placed on different coating properties, as well as the applicability and standardization of the various methods used to measure these properties. This milestone report provides an initial assessment of the most important coating properties and the experimental methods available for their determination to lay the foundation for standardized reporting and development of comprehensive datasets for modeling efforts. This report has determined that the residual stress of the coating is the most crucial property to investigate, yet it has received minimal attention to date due to a knowledge gap about the growth and formation of the brittle Laves phase under reactor conditions. The significance of residual stress of the coating is further enhanced by its connection and interdependence with other important properties like creep and coating failure mechanisms. This milestone proposes an importance rating for residual stress properties and their associated measurement techniques to fill in knowledge. Furthermore, techniques to investigate the outlined properties are discussed, and their capabilities and limitations are illustrated to provide guidance on their use.

CONTENTS

SUMMARY iii

1. INTRODUCTION 1

2. IMPORTANT PROPERTIES 4
   - 2.1 Thermal Expansion and Residual Stress 4
     - 2.1.1 X-ray Diffraction (XRD) 4
   - 2.2 Eutectic Penetration / Penetration Rate 6
   - 2.3 Thermal Creep / Irradiation Creep 8
     - 2.3.1 Nanoindentation 11
   - 2.4 Failure Mechanism (Cracking/Delamination) 12
     - 2.4.1 Nanoindentation 12
     - 2.4.2 Cantilever Testing 13
     - 2.4.3 Scratch Test 14
     - 2.4.4 Pull-Off Tests 15
   - 2.5 Plastic Deformation 15
   - 2.6 Thermal Conductivity 16
     - 2.6.1 Laser Flash Analysis (LFA) 17
     - 2.6.2 Thermoreflectance (TR) 17
   - 2.7 Irradiation Swelling 18
   - 2.8 Oxidation 19
   - 2.9 Elastic Modulus 20
   - 2.10 Specific Heat Capacity 20

3. SUMMARY 21

4. REFERENCES 22

FIGURES

Figure 1 Generalized Structure Zone Diagram [11]. 2

Figure 2 Fundamentals of the stress calculations using the $\sin^2 \psi$ method. L_3 is the normal to the diffraction planes and is in the same plane as the surface direction S_ϕ and the incident and diffracted beams (I_0 and I_D). S_1 and S_2 are vectors on the surface of the sample [23]. 5

Figure 3 The binary Cr-Zr system [28,32]. 7

Figure 4 TEM techniques: (a) EFTEM map, (b) EDS line scan across the interface [18] 7

Figure 5 Schematic of PT for creep study 9

Figure 6 Irradiation capsule or “rabbit” assembly used for placing coated rodlets in HFIR. 10

Figure 7 6 mm Keyence imaging configuration with vertical and rotational stage. 10

Figure 8 Schematic plot of a load-displacement curve obtained from nanoindentation [40]. 11

Figure 9 Deformation of a pure Cr coating versus buckling of a multilayer Cr/CrN coating after microindentation [45]. 13

Figure 10 Schematic plot of micro-cantilever testing [7]. 14

Figure 11 Bending failure of pure cathodic arc deposited Cr coatings [7]. 14

Figure 12 Scratch test results HiPIMS and cathodic arc deposited Cr, CrN/Cr, and Ti/Cr coatings on CVD SiC. Coatings with brittle layers showed brittle failure modes [45]. 15

Figure 13 Instrument setup of a NanoTR apparatus [62]. 18

Figure 14 TEM image of Cr coating shown with an under-focus of 0.5 μm [20]. 19

TABLES

Table 1 Summary of important properties of coatings and their investigation methods. 3

ACRONYMS

AOO	anticipated operational occurrences
ASTM	American Society for Testing and Materials
ATF	accident-tolerant fuel
BCC	base centered cubic
BISON	a finite element–based nuclear fuel performance code
BWR	boiling water reactor
CTE	coefficient of thermal expansion
CVD	chemical vapor deposition
DFD	dynamic force distribution
DSC	differential scanning calorimetry
EBSD	electron backscatter diffraction
EDS	energy-dispersive x-ray spectroscopy
EFTEM	energy-filtered transmission electron microscopy
FEM	finite element method
GTR	grid-to-rod
HFIR	High Flux Isotope Reactor
HiPIMS	high-power impulse magnetron sputtering
IFEL	Irradiated Fuels Examination Facility
LFA	laser flash analysis
LOCA	loss-of-coolant accident
LWR	light-water reactor
M5	zirconium alloy with 1% niobium developed by AREVA
MBT	modified burst test
ORNL	Oak Ridge National Laboratory
PCMI	pellet-clad mechanical interaction
PT	pressurized tubes
PVD	physical vapor deposition
PWR	pressurized water reactor
RIA	reactivity-initiated accident
SATS	Severe Accident Test Station
SEM	scanning electron microscopy
STEM	scanning transmission electron microscopy
TEM	transmission electron microscopy
TR	thermoreflectance
UTS	ultimate tensile strength
XRD	x-ray diffraction
YAG	yttrium-aluminum garnet
YS	yield strength
ZIRLO	advanced zirconium-based alloy by Westinghouse

DEVELOPMENT OF STANDARDIZED PROPERTY REQUIREMENTS, MEASUREMENT METHODS, AND REPORTING GUIDANCE FOR COATINGS

1. INTRODUCTION

Zirconium has been used as a fuel cladding material for over four decades but became subject to critical scrutiny due to the Fukushima-Daiichi loss-of-coolant accident (LOCA) in 2011. Traditionally, Zircaloy-2 was used in boiling water reactors (BWRs), while Zircaloy-4 was used in pressurized water reactors (PWRs). The cause of the accident can be found in the poor oxidation resistance of the cladding, leading to a loss of cladding integrity. This in turn can cause core relocation and release of fissile material. These findings led to the research on accident tolerant fuels (ATF) [1–3]. One of the most promising approaches to enhance the high-temperature behavior of the cladding is to apply a thin coating of highly corrosion-resistant material on the cladding's surface which does not interfere with the neutronic or mechanical performance of the base cladding under normal operating conditions. These coated cladding concepts have been tested in various ways to establish their limits and to ensure safe operation in nuclear reactors. However, different coating materials, thicknesses, coating processes, process parameters, and testing methods have an impact on the microstructure and mechanical properties and therefore on the results of the applied investigation methods, which makes the licensing of a selected coating cumbersome [4]. A large variety of methods has been developed to investigate coatings for cladding materials and their mechanical properties [5–9]. Coating performance must be evaluated with respect to the applied coating technique. For instance, physical vapor deposition coatings can have a thickness ranging from that of a single layer of atoms to several microns, whereas thermal spraying creates coatings with thicknesses ranging from 20 microns to several millimeters. In physical vapor deposition coatings, the adherence and uniformity of the coating is of utmost importance, whereas the maximum size of the defects is crucial when considering thermally sprayed coating. To improve the process, critical material properties must be evaluated and gathered to inform the certification process of cladding with a thin layer of a distinct unlicensed coating. For licensing purposes, standard materials testing is key. In this regard, each testing method must be assessed to define its advantages, disadvantages, and limits to provide the necessary data required for modeling and simulations [10].

This report focuses on investigation of methods applicable to thin coatings with thicknesses ranging from 5–50 μm as created by physical vapor deposition (PVD), since minimizing the added thickness to a licensed Zr-based cladding keeps the added neutron absorption low. Chromium is referenced as the coating material when the techniques are discussed because it is the most familiar coating proposed at this writing. A small thickness of a coating presumably limits the impact on the thoroughly studied Zr-based cladding properties during operation, and it also limits the possible accident scenarios. Furthermore, minimal thickness also provides a good corrosion resistance under normal operating temperatures and a good oxidation resistance under accident conditions. The process parameters to grow dense, mechanically adherent coatings using different PVD techniques such as the cathodic arc or the HiPIMS are important to investigate, but they are not different than the parameters used to grow coatings on non-cladding materials. Figure 1 shows the coating morphology based on the substrate temperature, kinetic energy of ions, and the deposition rate [11], and it also demonstrates an understanding of how the coating morphology can be tailored so that it excels in crucial areas such as the residual stress state of the coating and thermal and irradiation creep. Even though theoretical knowledge is available, application-relevant testing of coated claddings in reactor-relevant environments has been minimal so far [9,10,12,13]. Because tests in a nuclear test reactor like the High Flux Isotope Reactor (HFIR) at Oak Ridge National

Laboratory (ORNL) are time consuming and expensive, and because that type of test only creates a single data point of a single chemical composition and morphology, it is important to pinpoint the knowledge gaps for the most crucial coating properties.

These knowledge gaps are not limited to the sparse information about coating properties on cladding materials; they are also caused by the small amount of available testing methods applicable to irradiated materials and reactor-relevant geometries.

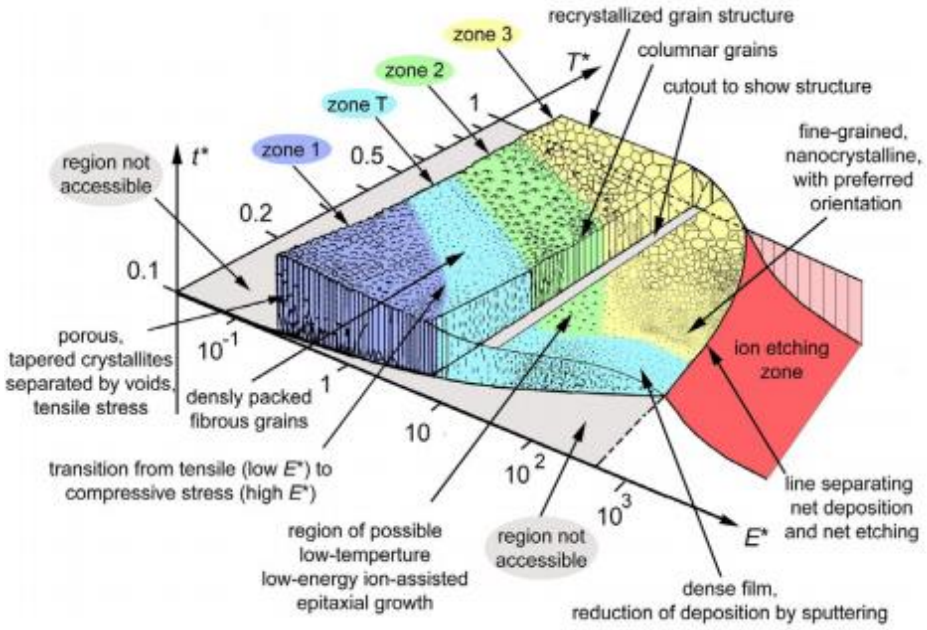

Figure 1. Generalized Structure Zone Diagram *[11]*.

To overcome these knowledge gaps, all relevant material properties for coatings on certified claddings were identified, evaluated, and ranked according to their importance to determine accurate simulations and certification in Table 1. This table provides an importance scale which ranks the most crucial properties and their investigation techniques according to an importance rating of 1 or 2. These properties and their investigation techniques exhibit significant knowledge gaps; ORNL and other research institutes must invest resources in the immediate future to overcome information gaps and to develop new testing techniques. On the other end of the importance spectrum is a rating of 10, which represents properties with sufficient information and testing techniques available. These properties, like elastic modulus and specific heat, are necessary for simulations and are used for elastic stress calculations, but they are either already well researched and known, or they have been determined to be of no concern in relation to certification and safety. The most important properties are thermal expansion and residual stresses, followed by eutectic penetration and creep.

As an illustration, note that thermal expansion and residual stress are ranked higher than steam oxidation of irradiated coating or creep properties caused by the unknown interplay of irradiation, temperature, corrosion, different thermal expansion coefficients, and heat gradient on the interphase. Residual stress outranks the aforementioned properties because of the current state of the knowledge gap and the important role it plays, since residual stress can lead to coating failure.

The following sections discuss the properties listed in Table 1 in order of descending importance. The available information and the most pressing concerns for each property are highlighted in each section, and the advantages and disadvantages of the main investigation techniques are evaluated.

Table 1. Summary of important properties of coatings and their investigation methods.

Importance[a]	Property	Technique
1	Thermal expansion / residual stress	XRD[b], indentation
2	Eutectic penetration / penetration rate	SEM[c], TEM[d], XRD
2	Thermal creep / irradiation creep	Creep tests, nanoindentation
3	Failure mechanism (cracking / delamination)	Nanoindentation, Scratch and pull-off test, cantilever bending, LOCA tests
4	Plastic deformation	Nanoindentation, XRD, Tensile tests, TEM, EBSD[e]
6	Thermal conductivity	Laser flash analysis, thermography
8	Irradiation swelling	TEM, STEM[f]
8	Oxidation	LOCA tests, SEM, TEM
10	Elastic modulus	Nanoindentation
10	Specific heat	DSC[g]

[a]Importance = 1 is highest, 10 is lowest
[b]XRD = x-ray diffraction
[c]SEM = scanning electron microscopy
[d]TEM = transmission electron microscopy
[e]EBSD = electron backscatter diffraction
[f]STEM = scanning transmission electron microscopy
[g]DSC = differential scanning calorimetry

2. IMPORTANT PROPERTIES

2.1 Thermal Expansion and Residual Stress

During the coating process, stresses are introduced into the coating caused by differences in thermal expansion at elevated temperatures and any occurring thermal gradients from the substrate to the coating. These stresses and strains can be beneficial by maintaining good process control during PVD to achieve a compressive stress inside the coating. This offsets and reduces the occurrence of crack-opening tensile stresses and spallation during operation. The PVD process achieves strong mechanical bonding of coating and substrate, which is beneficial for delamination or spallation, but it could have a negative impact on the strain and stress at elevated temperatures during normal operation inside a reactor. This occurs because of different thermal expansion coefficients between a Zr-based cladding and a chromium coating. During normal operation, differences in the thermal expansions of Cr and Zr at operating temperature will cause stresses in the coating. However, the coating stress state can be very sensitive during temperature changes based on the difference in cladding and application temperatures resulting from the higher thermal expansion coefficient of Cr (8.95×10^{-6} m/m) compared to that of Zircaloy (6.0×10^{-6} m/m) at light-water reactor (LWR) operating temperatures [14,15].

The formation of the Cr_2Zr Laves phase was observed and investigated at transient temperature ranges of 600–1200°C. The thickness of the layer was found to be around 0.1 and 0.3 μm under normal operating conditions, and it grew up to 7 μm in case of a long-term loss-of-coolant over 1 day at 800–1200°C) [16]. The microstructure, yield stress, hardness, oxidation behavior and fracture toughness of the Laves phase has been investigated [17,18] to determine its potential impact on the cladding material. The residual stress that was induced due to the different thermal expansion coefficient of this brittle intermetallic phase—the Zr-based cladding and the Cr and Cr_2O_3 layer—can lead to microcracking at the interface [19]. The stress state of the coating is also affected by other phenomena, such as irradiation swelling and the diffusion kinetics. Irradiation swelling of the coating can introduce voids inside the coating which change the stress state of the coating [20]. In addition, the diffusion kinetics and the thickness of the coating should be investigated to analyze the interdiffusion of Cr and Zr and the formation and growth of the Laves phase and to quantify their impact on the longevity of the coated cladding. Therefore, residual stresses must be identified so that the development of strain and stresses of the coating during operation can be simulated and analyzed. XRD methods are the most common techniques used to investigate residual stresses. They can be applied before and after irradiation to coated cladding tubes to provide ex situ data points for simulation purposes.

Cutting-edge in-situ strain and stress measurements of heated tubes with thermal barrier coatings used for turbine blades using synchrotron x-ray diffraction have recently shown the importance of providing data on the stress state of coatings for certification and simulation during operation [21]. However, those techniques cannot be used to simulate in-situ reactor conditions and do not enhance knowledge of coated cladding materials for this work. Therefore, it is recommended that easily applicable XRD residual stress measurements be performed on coated cladding material.

2.1.1 X-ray Diffraction (XRD)

Stresses are categorized into microscopic and macroscopic stresses [22]. Microscopic stresses result from imperfections in the crystal lattice, and the distance they extend is smaller than the dimension of a single crystal. On the other hand, macroscopic stresses extend over several grains and are important for design and failure analysis. Both stresses can be measured indirectly using XRD methods by determining the breadth of a diffraction-peak position for microscopic stress and the shift of a diffraction-peak position for macroscopic stress. The stress cannot be measured directly—instead, the strain of the lattice is determined using Bragg's equation to calculate the macroscopic stress. A shallow depth of the x-ray penetration of only a few microns accommodates the assumption of zero stresses in the normal direction of the surface,

with the assumption of the coating being in the state of plane stress only. This approach simplifies the stress-strain equation and eliminates the need to know the lattice distance in the non-strained condition. However, Poisson's ratio ν and the geometry of tubes can lead to strain and stresses in the normal direction of the plane [23]. A carefully aligned collimator and a parallel beam setup [24] are recommended to collect reliable data. A standard of the non-strained condition is not necessary due to the application of the $\sin^2 \psi$ method, where ψ is the angle between the normal of the surface S_3 and the bisector L_3 of the incident and diffracted beam, as shown in Figure 2.

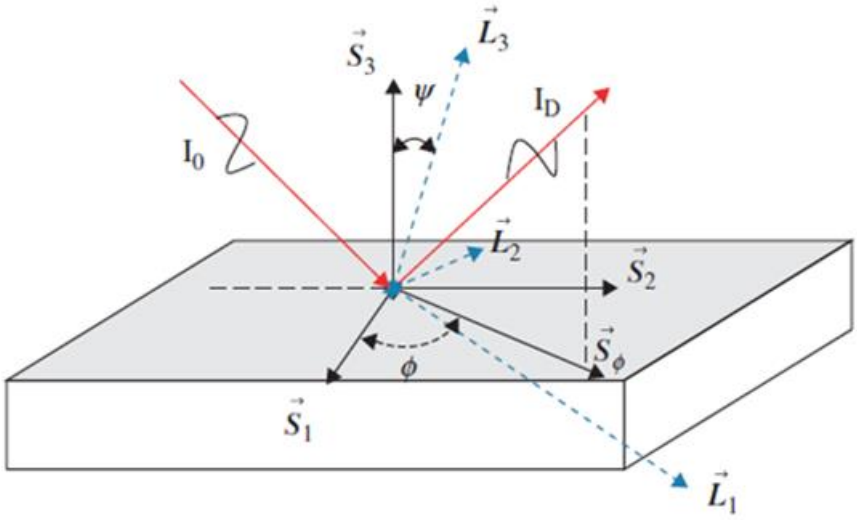

Figure 2. Fundamentals of stress calculations using the $\sin^2 \psi$ method. L_3 is the normal to the diffraction planes and is in the same plane as the surface direction S_ϕ and the incident and diffracted beams (I_0 and I_D). S_1 and S_2 are vectors on the surface of the sample *[23]*.

The elastic strain can then be calculated using the following relationship under the assumption that a bi-axial stress state exists in the surface plane, with zero stresses in the normal direction to that plane:

$$d_\psi = \left(\frac{1+\nu}{E}\right) d_\phi \sin^2 \psi - \frac{\nu}{E} (\sigma_{11} + \sigma_{22}) d_0 + d_0,$$

with an elastic surface stress σ_ϕ along the S_ϕ direction of

$$\sigma_\phi = \sigma_{11} \cos^2 \phi + \sigma_{12} \sin 2\phi + \sigma_{22} \sin^2 \phi,$$

where E as the elastic constant, ν is Poisson's ratio, d_0 is the non-stressed lattice parameter, and σ_{xy} is the stress components of the stress tensor. The slope of a plot of d_ψ vs. $\sin^2\psi$, where d_ψ is assumed to be equal to $d_{\psi=0}$, delivers the stress along the S_ϕ direction, if E and ν are known [23,25]. This method, known as the *$\sin^2\psi$ technique*, is easy to apply to a coating of only a few microns and can also be applied to irradiated material, which makes this nondestructive technique a valuable tool when determining the residual stress inside the coating before and after irradiation [20]. However, it is important to note that the calculations become more difficult if the strain values in the normal direction of the surface plane are not zero. A reasonable way to determine whether stress in the normal direction should be considered is to check whether the slope of the plot of d_ψ vs $\sin^2\psi$ is linear. If that is not the case, then the strain values for that direction must also be included in the analysis.

Due to the limited energy of the x-ray radiation, the coating thickness for this method is limited to ≈25 microns. The measurements cannot be performed in situ, which can make it difficult to distinguish between thermal- and irradiation-induced stresses. The elastic modulus for the different lattice planes

must be known, and the possible anisotropy of the coating must be identified using EBSD techniques. An advantage of this technique is that it is not necessary to prepare the sample surface prior to using the nondestructive XRD method. An additional advantage of this method is that irradiation-induced strain will be visible in the stress analysis after irradiation, providing valuable information for a database. Therefore, it is highly recommended that the $\sin^2\psi$ method be applied for analysis of coatings before and after irradiation.

Other techniques that are reliable for collecting information about the residual stress inside the coatings—like grazing angle XRD and wave curvature laser transducer methods—are also recommended as complementary methods to be applied [24]. Wave curvature laser transducer methods are especially helpful for providing in-situ stress measurement while the coating is grown [26]. Nanoindentation for measurement of residual stress is also a possible option, but it needs to be performed in addition to finite element method simulations to provide reliable data [27]. Therefore, XRD methods are preferred and highly recommended.

2.2 Eutectic Penetration / Penetration Rate

The binary system of Cr-Zr is shown in Figure 3 [28]. Elemental chromium and zirconium have very high melting points of 1907 and 1855°C, respectively, but the phase diagram shows two eutectics with eutectic temperatures of 1559°C on the Cr-rich side and 1316°C on the Zr-rich side, which limit the maximum temperature at which a Cr-coating on a Zr-based cladding could endure. Even though pure chromium is grown on the Zr-based cladding, formation of the intermetallic Laves phase Cr_2Zr on the interface and diffusion of both elements require careful assessment of temperature limits for a modeling approach. Penetration of Cr-Zr intermetallic may change the structural properties of Zr cladding. These changes could be caused by irradiation, temperature cycling, and/or accident scenarios and are typically not modeled, but they may be crucial to be incorporated. Determining changes on the interface requires visual investigation of the edge cases of thermal treatments of coated cladding at LOCA-relevant temperatures and after integral LOCA tests on high-burnup fuel segments [29,30]. ORNL provides excellent conditions to perform these tests using the Severe Accident Test Station (SATS) in the Irradiated Fuels Examination Facility (IFEL). At SATS, testing of irradiated samples even beyond LOCA conditions can rapidly generate data. This is accomplished by applying SEM methods to investigate phase changes using electron backscatter diffraction (EBSD) in combination with nanoindentation [7].

TEM methods are used to determine the changes of the Laves phase by using electron diffraction patterns of the atomic lattice and EDS line scans [7,18]. An energy-filtered TEM (EFTEM) map and an EDS line scan result are shown in Figure 4 [18]. These methods are clearly capable of measuring and analyzing the growth and size of the Laves phase, which is a crucial step when determining the lifetime and the limits of coated claddings. Additional investigation may be necessary to determine the compatibility between materials under irradiation and how this impacts the cladding substrate properties, but the aforementioned techniques should be applied and evaluated first.

If the Cr_2O_3 layer grows substantially during operation, then the ternary phase diagram of Zr-Cr-O should be examined to determine the locations and temperatures of the eutectics. However, initial studies show that chromium forms a 100–300 nm layer of chromia at 300°C in LWR conditions [31].

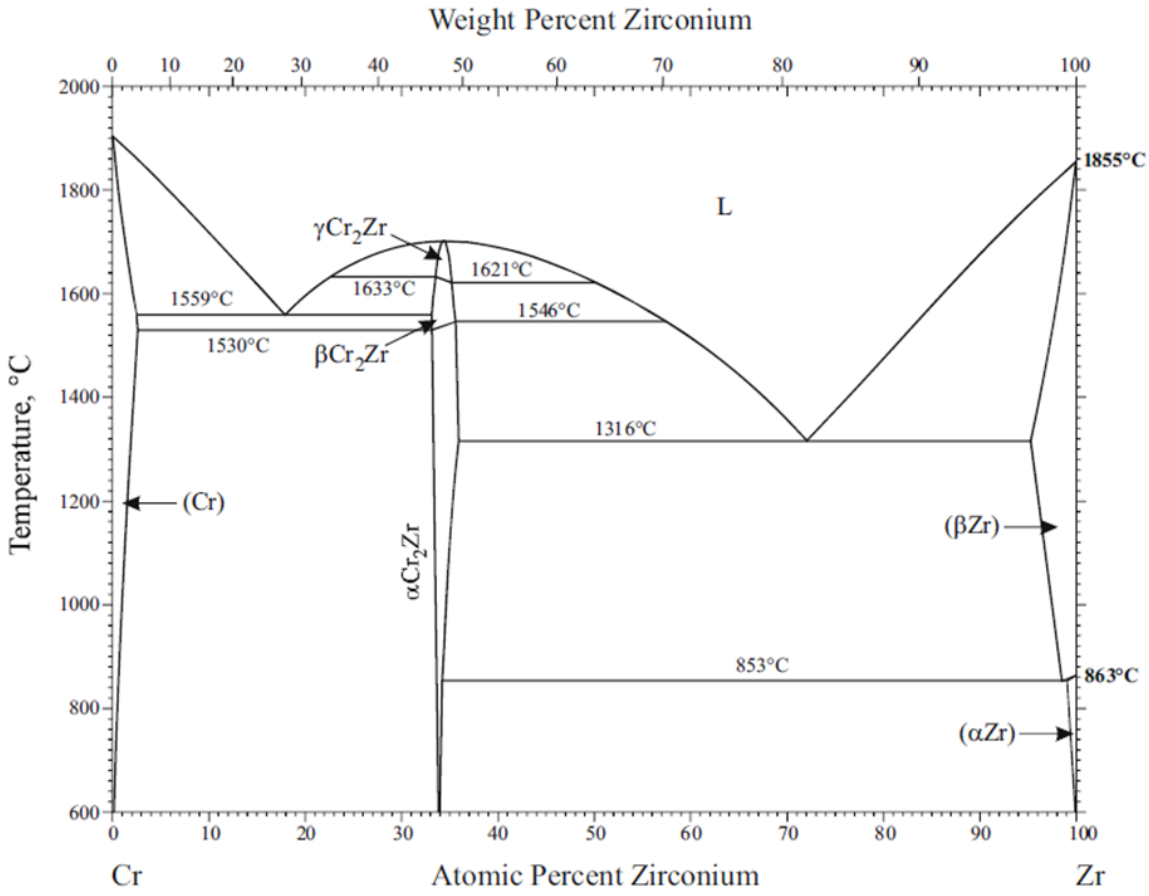

Figure 3. The binary Cr-Zr system *[28,32]*.

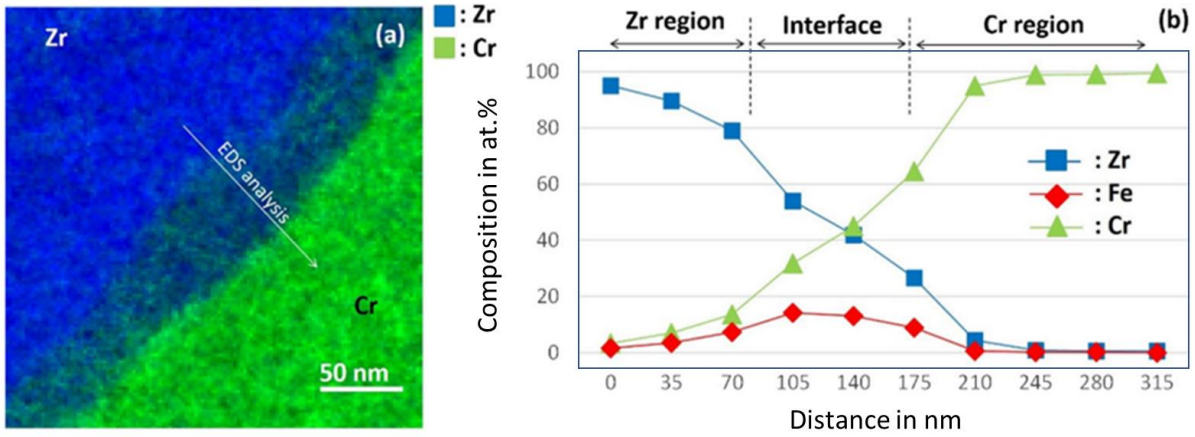

Figure 4. TEM techniques: (a) EFTEM map, (b) EDS line scan across the interface *[18]*.

2.3 Thermal Creep / Irradiation Creep

In an LWR (both PWR and BWR), the fuel cladding is under an external pressure from the reactor coolant system and an internal pressure due to internal gas, which includes fill gas added at manufacture and fission gas released during operation. Because the external pressure is significantly greater, the cladding and fuel achieve pellet-clad mechanical interaction (PCMI) as the cladding slowly creeps down around the fuel. Thermal expansion of the fuel pellets and pellet swelling expand the fuel and subsequently the cladding, leading to radial expansion of the cladding in both reactor types. The cladding slowly relieves stresses formed during this expansion through a combination of thermal and irradiation creep. Additionally, PCMI can stress the cladding in the axial dimension. These mechanisms are well researched, and creep deformation is established and accounted for in Zr-based cladding [33]. The total creep deformation is the sum of irradiation creep and thermal creep deformation. Initially, the thermal creep deformation is the dominant factor in Zr-based alloys. However, due to irradiation hardening, the thermal creep contribution quickly diminishes to around 10% of the total creep deformation, and the irradiation creep deformation becomes dominant. Thermal creep data for pure Cr are available and described well using a Norton creep law [10], but the growing oxide layer and the Laves phase are not represented in that data.

The presence of a coating may alter the above-mentioned behavior if the coating material inherently shows lower strain-hardening rates than the cladding material. This could lead to large stresses on the interface at the location of the brittle Laves phase. If the stress increases above the van Mises yield criterion, then plastic deformation, spallation, and/or delamination of the coating could occur. Due to the limited plastic deformation of the Laves phase, critical failure of the coating could occur. In addition, the coating's thickness could impact the strain hardening rates, which makes the thickness of coatings a more relevant parameter to investigate.

Understanding the role of creep on coating behavior is important for two primary reasons. First, the inability of applied coatings to deform if the cladding substrate creeps during service may impair their performance during service and off-normal conditions. The main concern is that the creep of the cladding material would impact the coating stress state and could encourage crack opening. In this effort, it is important to verify that the coating can withstand the creep-induced tensile stresses. The second reason that creep coating behavior is important is that the presence of a coating may impact the deformation behavior of the coating as a function of time. The coating diameter, and more specifically the fuel-clad gap dimension, is a critical parameter that dictates numerous critical parameters, including fuel centerline temperature and internal rod pressure [34]. In general, it is unlikely that the coating will impact the thermal creep of the composite cladding material, because the thickness of the coating is relatively small in comparison to the cladding. However, significantly lower thermal and irradiation creep strain may prevent cladding creepdown to some degree. Data on the thermal creep of chromium show creep strain rates 4× lower than Zircaloy at ~1100K [35,36]. Extrapolating this data to coolant temperatures during operation (600K) leads to estimations of ~10^5× less thermal creep deformation in the chromium coating. Likewise, the irradiation creep rate for chromium metal, if estimated to be similar to iron-based BCC steels, is expected to be near 10^2× less than that of Zr-based cladding [36,37]. These creep rates are also expected to be highly dependent on the microstructure of the applied coating.

The decreased creep rate of the coating may allow the coating to support some of the hydrostatic pressure from the coolant for longer periods of time, which subsequently reduces the stress on the cladding. With less stress, the cladding will undergo less creepdown. Understanding and modeling the cladding stress state as a function of service time and, in turn, its impact on cladding dimensions is therefore an important issue relevant to licensure and performance. To date, the only practical way that the role of coatings on irradiation creep has been studied is through post irradiation examination of integral tests or more recently dedicated rabbit irradiations performed in HFIR using pressured tubes. Use of integral tests, performed either in test reactors such as ATR or commercial reactors, provides representative conditions including

the evolution of stress state as a function of service time. However, collecting data in this manner is expensive, time consuming, and provides only a single data point with respect to a coating geometry and reactor time. Further, the numerous effects acting in concert to drive change in cladding dimension may be difficult to deconvolute. Alternatively, use of HFIR to irradiate pressurized tubes to obtain irradiation creep data has been demonstrated for structural materials [38] and recently deployed successfully for coated zirconium tubes [39]. The advantages of this approach are the more rapid accumulation of data (~2 dpa per HFIR cycle) and ability to field a more diverse matrix of stress states and coating thicknesses than possible in an integral test. This lends the methodology to studies specifically aimed at benchmarking models through a Separate Effects approach.

Pressurized tubes (PTs) were fabricated according to the design outlined by Mulligan et al [38]. The thin-walled tube section had an outer diameter of 4.57 mm and was 25.4 mm long with a 0.255 mm nominal wall thickness in Figure 5. A SiC tube is placed inside the PT capsule to provide passive temperature measurement and to displace free volume to reduce the mass of high-pressure gas.

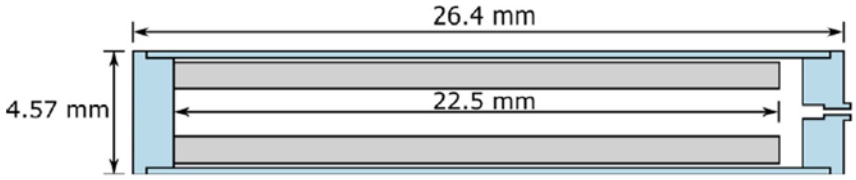

Figure 5. Schematic of PT for creep study.

Tubes are fabricated from bar stock composed of the desired base zirconium alloy (e.g. Zry-2, Zry-4, or advanced commercial zirconium alloys such as ZIRLO or M5) using conventional drilling and lathe machining techniques. Following machining, endcaps are welded to the tubes using an e-beam welder. These tubes can then be coated with the desired coatings. Finally, the rodlets are internally pressurized with ultra-pure helium by placing the assembly in a high-pressure chamber and sealing with a 400 W pulsed Nd:YAG laser.

Following rodlet coating and pressurization, test specimens are assembled with other support components to create irradiation capsules, as shown in Figure 6. Temperatures in the capsule are controlled via small insulating gas gaps between the holder and aluminum housing that was in contact with the HFIR coolant. Precise machining of these gaps and selection of an inert fill gas with a desired thermal conductivity are critical to achieving design temperatures in the rodlet.

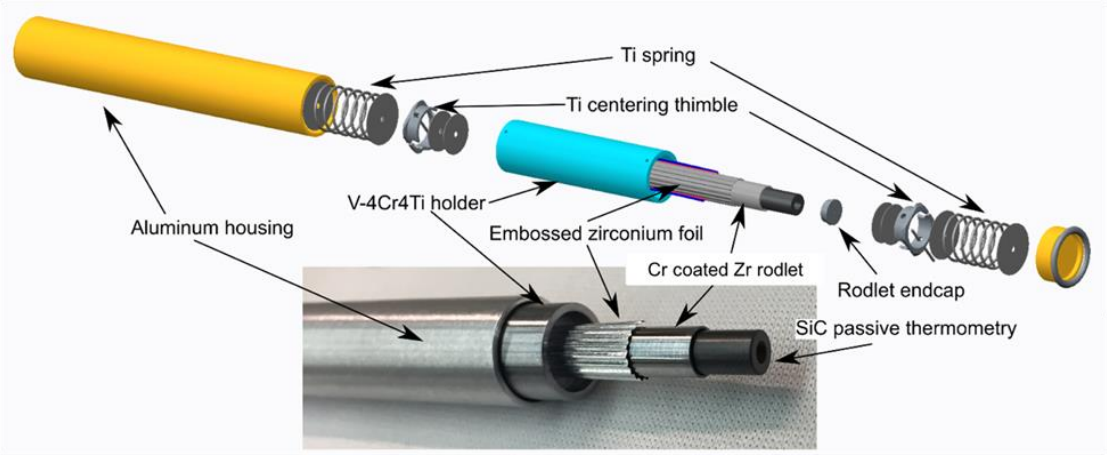

Figure 6. Irradiation capsule or "rabbit" assembly used for placing coated rodlets in HFIR.

Pressurized tube experiments are an established method for measuring material creep; however, the technique used for measuring dimensional changes in irradiated PTs is still evolving. The ability to capture dimensional changes on the order of micrometers is critical. In this particular application of material creep measurement, it is also paramount that any technique is capable of being replicated in a hot cell environment, where measurements are conducted in a closed chamber in a harsh radiation environment several meters from the operator using remote manipulators. The current method in use by ORNL uses laser profilometry performed using both vertical and rotational stages that can be deployed in cell. A photograph of this method as deployed out of cell is shown in Figure 7. Accurate measurement of sample diameters before and after irradiation then provides a dataset from which irradiation creep can be determined.

Figure 7. 6 mm Keyence imaging configuration with vertical and rotational stage.

While this method provides a means of acquiring data on the impact of a candidate coating on irradiation creep far more rapidly than integral tests. The outcome remains data that summarizes the composite response of the coated cladding. Data obtained in this manner may be adequate to make the claim that a

coating does not impact irradiation creep of the base zirconium alloy, but it will be difficult to use these datasets to quantify measurable impacts or inform models that could be used to predict coating impacts if the coating thickness varied or reactor temperature increased. Surface investigation techniques like nanoindentation of the coating and could help identify the creep data of the coating itself.

2.3.1 Nanoindentation

Nanoindentation methods can be used are used to determine creep properties of coatings. A small tip often in the shape of a 4-sided pyramid, called a Berkovich indenter, is pressed into the surface and load-displacement curves can be recorded. Figure 8 shows a typical load-displacement curve obtained from nanoindentation [40]. This type of conventional nanoindentation is used in a an open-loop method, which utilizes voltage applied for a fixed time period to generate the required load for the indentation. That approach does not correct and account for the spring in the transducer which absorbs a small portion of the load [8]. Therefore, no constant load can be applied when holding a peak load, which presents great challenges in doing creep studies. For that reason, it is recommended to use closed-loop load controlled or displacement controlled [41].

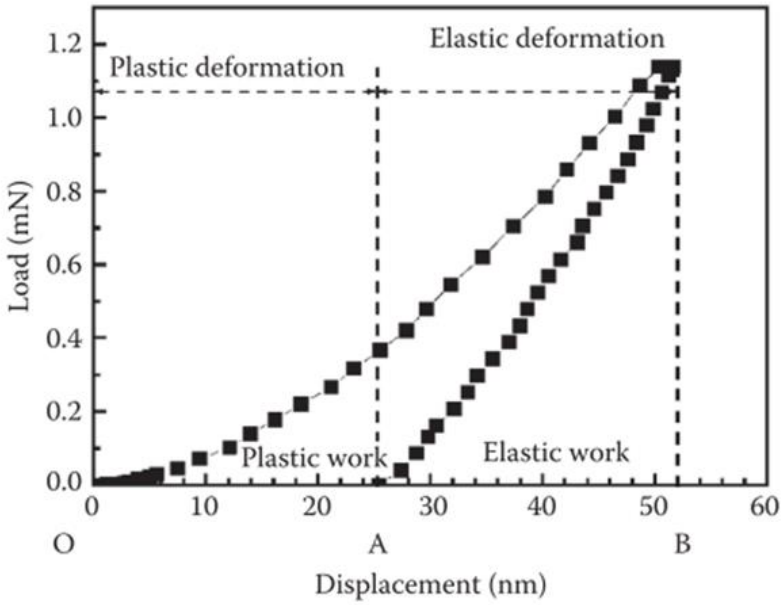

Figure 8. Schematic plot of a load-displacement curve obtained from nanoindentation *[40]*.

However, it is necessary to mention first, that indentation creep experiments performed with a nanoindenter are difficult to compare to results obtained from uniaxial creep tests with a steady state microstructure and a constant stress. Indentation of a coating causes strong work hardening and because of that, it extends the primal creep processes. Furthermore, the indenter shape has a strong impact on the mean contact pressure, which declines over time due to the stress relaxation of the material around the indenter, even though the load on the contact is kept constant. In addition, the localized strain field and the deformed volume can redistribute, which is impossible using uniaxial creep tests. That means that the results cannot easily analyzed using steady-state creep regimes [42]. For that reason, the nanoindentation creep experiments should be rather considered to be load relaxation tests. Steady-state creep-rates are very well described using the expression [40]:

$$\dot{\varepsilon} = K\sigma^{n} = K\sigma^{1/m}$$

with n as the stress exponent, m the strain-rate sensitivity and K as a constant.
Knowing that, Takagi et al [43] were able to find conversion coefficients for extracting uniaxial creep data from pseudo-steady indentation creep tests results using finite element simulations for n=2-7 for an Aluminum alloy to convert strain rates extracted from nanoindentation to values comparable to those found for steady-state creep. However, the performed tests were not performed on coatings and were without the consideration of the substrate. For thin coatings on cladding, the substrate will impact the creep test data significantly.

That means, that creep tests using a nanoindenter are possible, but the acquired data needs to be carefully analyzed, due to the mentioned caveats. Conversion factors found by Takagi et al [43] would need to be tested and verified by FEM simulations and extensive creep experiments. Durst et al [42] published a highly recommended publication, which should be the basis for every approach towards creep tests and the controversially discussed topic what nanoindentation is able to deliver in regards to long term creep test using nanoindentation and the collection of data.

2.4 Failure Mechanism (Cracking/Delamination)

It is necessary to investigate the limitations of the strength of the coating–cladding adherence to determine if the coating will delaminate or crack under normal operation and heat cycling. In addition, the hardness and wear resistance need to be determined due to the possibility of GTR fretting in the reactor. Cracking, but no delamination has been observed at 4%-6% strain on coated M5 samples. For certification and modeling approaches, it is inevitable to assess a failure criterion during operation/burst. For that reason, nanoindentation, microcantilever and scratch tests need to be performed. Pull off tests are easily applicable to non-irradiated material but become more difficult with irradiated material due to the need of rather large samples and limited in their applied force. Information about the irradiation hardening behavior of pure Cr coatings are sparse and datapoints need to be created to enable accurate simulations [10]. No information is available about the irradiation behavior of the Laves phase and needs to be acquired to determine if the implementation of the Laves phase a separate layer in modeling approaches is needed. The required data can be acquired using indentation, cantilever and scratch test on the coating and the interphase after and before irradiation.

2.4.1 Nanoindentation

Nanoindentation will be the main instrument to determine the hardness values, the E-moduli and failure mechanisms of the Cr-coated Zircaloy. An ISO standard for nanoindentation was published in 2002 and should be followed for all measurements to determine data for modeling approaches [44]. Microindentation can be applied to both the surface, and the interface of coatings [40]. Surface indentation relies on the plastic deformation of both the substrate and coating by a Vickers, or other hardness indenter. This can result in the buckling and cracking of the coating. The relative ductile nature of Cr as compared to that of Zr-based alloys makes this test less applicable. If indents are made close to areas with visible spalling, cracks can be observed in the coatings. However, if indents are moved to more adherent regions, then deformation is observed in the coating, without buckling, spalling, or cracking as shown in Figure 9 [45]. Cross-sectional microindentation can be used to examine coating adhesion by placing the point of the indent at the coating/substrate interface [46]. The initiation and propagation of cracks along the interface can be used to determine the relative toughness of the coating interface. However, the use of microindentation is more suited for thicker coatings where the size of the indentation is small compared to the coating thickness. Nanoindentation has been applied to thin coatings of up to 1.3 μm on single crystal wafers [4]. The applicability of nanoindentation on towards the development of coatings on Zr-based cladding might be limited by the surface roughness of the substrate.

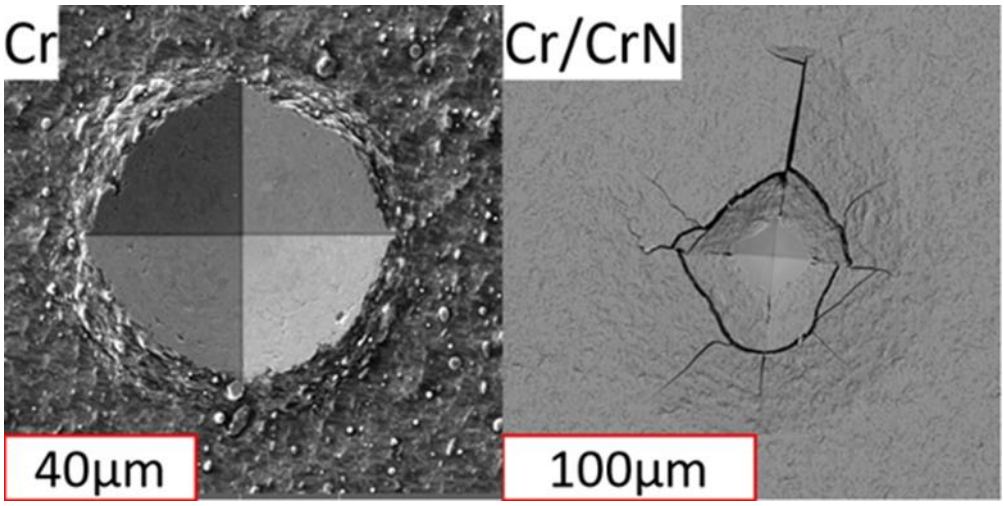

Figure 9. Deformation of a pure Cr coating versus buckling of a multilayer Cr/CrN coating after microindentation *[45]*.

Relatively smooth surfaces are needed for both surface nanoindentation as well as cross-sectional, while smoother surfaces are not as favorable for coating adhesion. An additional testing mode for cross-section indentation is placing the indent in the substrate near the coating. In hard/brittle substrates the indentation can create either cracks running towards the interface or cleave off a wedge or "shelf" of material. The creation of a shelf enables the testing of the adhesive strength as it effectively pushes out against the coating. This has been replicated in Cr coated SiC but was never subject to rigorous experiments as cohesive failure of the coating was more likely to occur. The creation of cracks is more useful in studying the effectiveness of the coating at maintaining hermeticity during substrate cracking. Several tests where cracks were initiated in the substrate have been conducted [45].

These demonstrated the ability for softer coatings to blunt and terminate cracks or deflect them at the interface, while hard ceramics coatings allowed the cracks to easily penetrate through. When shelving did occur, no large-scale adhesive pull-away of the coating was observed, but rather cohesive failures occurred. Since the tests were focused on inducing cracks and not shelves it is not clear if the high likely hood for cohesive failure was due to the strong adhesive nature of the coating, or improper geometry.

2.4.2 Cantilever Testing

Microcantilever testing isolates and tests the fracture strength of the coating, but also requires significant equipment and expertise [5]. From the standpoint of understanding and measuring the fundamental/idealized strength of a coating, this technique is the most direct. A focused ion beam is used to cut out a small cantilever leaving the coating/interface near the base of the pillar. The beam geometry requires coating thicknesses that are large enough to form a proper beam, while very thick coatings need to be cut down to keep the correct beam width to length ratio. Once cantilevers are formed, then an in-situ nanoindentation system in an SEM can be used to push down the beam and record the deflection and failure force. A schematic of the test setup for a tungsten coating on SiC is shown in Figure 10 [7]. For hard coatings, linear elastic beam mechanics can be used to calculate the force at the interface when failure occurs, however ductile samples are more complicated. Cr coatings deposited by cathodic arc have been observed to be sufficiently ductile to bend instead of break, as seen in Figure 11 [7]. This removed the ability for the test to measure the adhesion strength at the interface. However, the direct visualization of the ductility of the coating is still valuable information, and the maximum force at the interface before the bending can be calculated.

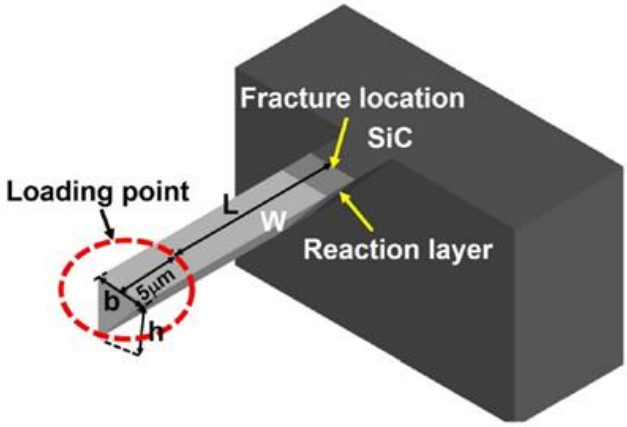

Figure 10. Schematic plot of micro-cantilever testing *[7]*.

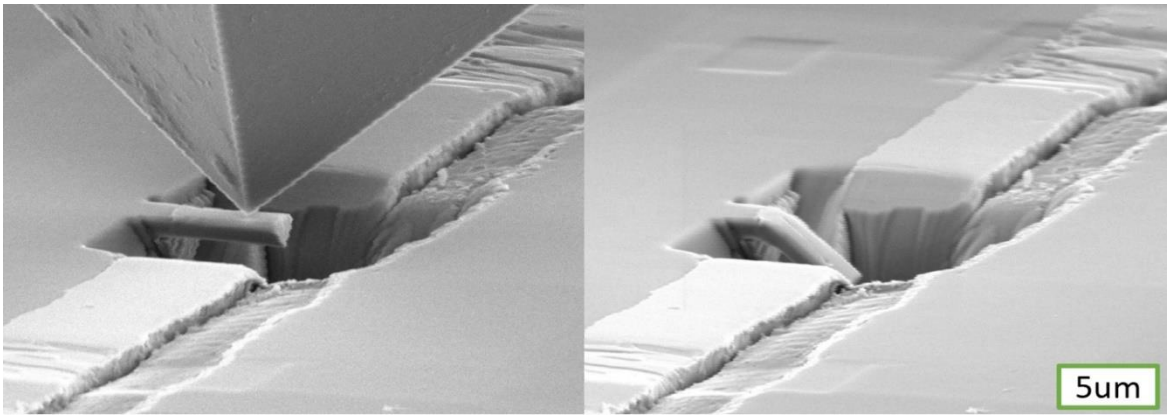

Figure 11. Bending failure of pure cathodic arc deposited Cr coatings *[7]*.

2.4.3 Scratch Test

Scratch testing is one of the most common test methods due to its relative ease and consistency. A tip is dragged at a set rate across the material with an increasing load. The visual failure of the coating can be correlated to the load and shear forces at the point of failure. Straightforward data analysis is limited by the need to have samples containing similar coating geometries/roughness as well as testing parameters. Coupling the visual and force feedback results with acoustic emission monitoring and finite element modeling can help provide more quantitative results but require more in-depth analysis. Once again, this technique is more effective on harder coatings on softer materials, with the ASTM C1624 standard designed for ceramic coatings. Since a large amount of shear forces can be imparted into the coating, scratch tests do add an additional testing mode as compared to an adhesion test which isolates an orthogonal force. It is not surprising that scratch testing of initial pure ceramic and multilayer ceramic/metallic coatings provided more standard and repeatable coating failures than that of pure metallic coating in Figure 12 [45]. Testing on ductile Cr coatings have shown that material plastically deforms but does not delaminate, with the indenter effectively spreading the coating along the surface of the sample. The plastic deformation limits the amount of shear force transmitted to the interface.

Scratch testing does not provide additional information on the mechanical robustness between the various relatively well adherent pure metal coatings as compared to other testing methods. The test does have its uses as the interface of weak ductile coatings will fail, as seen by the Ti/Cr coating. Cross-sectional

imaging of this coating type showed that the Ti layer was severely buckled after Cr was deposited on top causing the coating to spall during scratch tests, while pure Ti coatings did not show spallation.

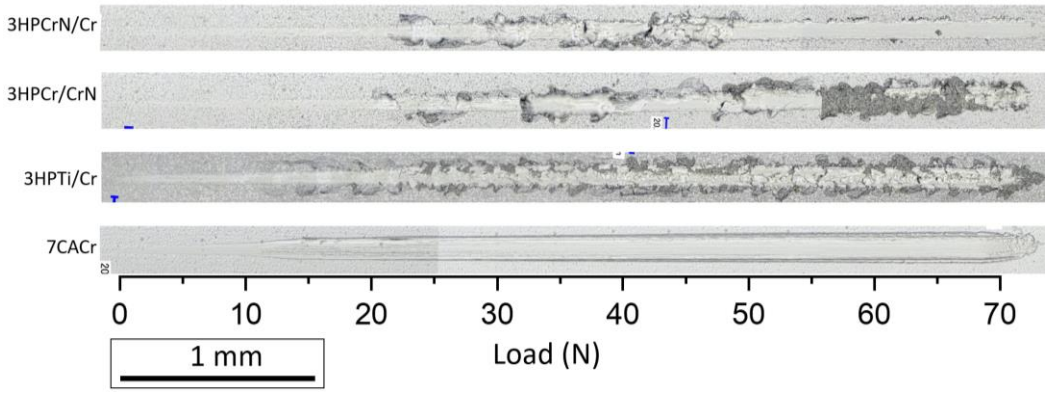

Figure 12. Scratch test results HiPIMS and cathodic arc deposited Cr, CrN/Cr, and Ti/Cr coatings on CVD SiC. Coatings with brittle layers showed brittle failure modes *[45]*.

2.4.4 Pull-Off Tests

Pull-off adhesion tests are very simple and can provide direct quantitative measurements. A testing stub is epoxied to the coated sample, and then the force required to pull off the stub is measured. There is an ASTM C633 standard for thermal spray coatings, which is designed for testing larger coating areas with a load frame. For testing smaller areas there are other devices such as the MICRO adhesion tester from DFD Instruments which is designed for use with 2.8mm diameter stubs. This limits the force needed to run the test, which is beneficial as smaller CVD SiC coupons can and will break easily.

Pull-off adhesion tests are limited to measuring up to the adhesion strength of the epoxy used to secure the pull-stub to the coating. However, if the testing device properly balances the load, the force required to pull off the coating can be directly measured. New thermoset epoxies have adhesive strengths up to ~85 MPa with proper bonding to the coating surface. Adhesion values in this range can be considered to be a sufficient, as thermal spray coatings have adhesive strengths in the 30-40MPa regime. When a coating failure occurs, it can either be a partial failure, where a small portion of the coating is removed, or a complete failure where all the coating that the epoxy is bonded to is removed. Partial failures make the analysis of the failure stress more complicated as the surface area changes. However, this localized adhesive failure also reveals the inhomogeneity in a coatings bond; macroscopic features that can be missed in micro scale testing. These tests are also limited to planar surfaces, which limits the usability of those tests to the process of coating development step, due to the tube shape of the coated cladding.

2.5 Plastic Deformation

The coating is required to plastically deform readily with the cladding during deformation from power ramps and transients due to its small thickness. Kim et al [47] performed Ring Tensile and Compression Tests on laser coated Zircaloy-4 cladding tubes in combination with cross-sectional SEM observations after 2, 4, and 6% strain. The Cr-coated layer with a thickness of around 50 μm cracked at more than 4% strain, but no spalling or peeling was visible. A high-temperature oxidation test at 1200 °C for 2000s was conducted but no spalling or peeling was detected either. These preliminary results are very positive, even though a different coating process was used, and the tested Cr layer was much thicker than a PVD coating.

Ribis et al. [13] performed a tensile test of Cr-coated Zr-4 alloy neutron irradiated at 350 °C (2dpa) and no delamination was found. For those reasons, the plastic deformation it is not ranked as one of the most crucial properties to investigate from a safety and certification standpoint. However, certain parameters and datapoints are missing and needed to simulate the plastic deformation of Cr-coated Zr-4 cladding. The impact of irradiation hardening needs to be determined and especially the ultimate elongation of the inherently brittle chromium needs to be recorded at different temperatures to implement deformation behavior at elevated temperatures.

Another factor to investigate is the substantially lower YS and UTS (~40%) of Cr in comparison to Zircaloy. However, the "Supplemental Guidance Regarding the Chromium-Coated Zirconium Alloy Fuel Cladding Accident Tolerant Fuel Concept" [48] stated, that the Cr coating is not meant to take part of the structural load of the cladding material and the cladding thickness cannot be decreased to make up for the added thickness of a coating. The plastic deformation inside the coating needs to be observed and measured to implement models to accurately describe and predict the behavior of the coating. To be able to measure the plastic deformation, nanoindentation methods on the coating need to be performed in axial and radial direction to determine the mechanical properties of the coating before and after irradiation. To determine the elastic response, the hardness, and the ability for plastic deformation of coatings most commonly nanoindentation of 4-sided pyramid shape into the material is used to record load-displacement curves. The plasticity index PI can be calculated by dividing the plastic deformation (OA) by the total deformation (OB) shown in Figure 8 in section 2.3.1 on page 11. Those curves can be analyzed to determine the indentation stress and strain [49].

Plastic deformation of metals is governed by dislocation motion, leading to the interaction of dislocations, storage, pile-up, and annihilation processes during plastic deformation at a given strain rate. For that reason, strain rate jump tests using nanoindentation as described by Durst et al [42] are recommended and nanoindentation should serve well to determine the plastic deformation of the coating.

2.6 Thermal Conductivity

A high thermal conductivity of the cladding material is important to dissipate the heat produced from the fuel during operation in a safe and effective way. The thermal conductivity of a coating and the formation of coating oxide may increase the cladding, and consequently, fuel temperatures. If significant, this may impact fuel fission gas release behavior and the cladding thermal creep behavior. Further issues may arise if the intermetallic formed between the cladding substrate and coating degrades heat transfer. The thermal conductivity of Cr is around 60 $Wm^{-1}K^{-1}$, around 12 $Wm^{-1}K^{-1}$ for Zr, and around 3 $Wm^{-1}K^{-1}$ for Cr_2O_3 [50–52]. Depending on the thickness of the Cr_2O_3 layer, the thermal conductivity could compromise heat transfer. However, the usually formed zirconia layer on the surface of the uncoated cladding provides a similar thermal conductivity of around 2.5 $Wm^{-1}K^{-1}$. Given that thermal conductivity of zirconium alloy cladding during operation does not incorporate a degradation term to correct for ZrO_2 formation during service, this phenomenon is not a primary concern.

A potentially important factor in context of the thermal conductivity is the relative penetration thickness of the intermetallic, a related potential embrittlement of the interphase, causing a delamination or spallation and a potential amorphization of the Laves phase, which was reported after ion irradiation [53]. These areas would exhibit a reduced thermal conductivity. Another important factor is the irradiation induced void formation, and introduction of dislocations, which further decrease the thermal conductivity.

The thermal conductivity $\lambda(T)$ can be calculated using the thermal expansion $\alpha(T)$, heat capacity $c_p(T)$ and thermal diffusivity $\mu(T)$. Common methods to determine these parameters are differential scanning calorimetry (DSC), differential dilatometer measurements or DSC, and laser flash analysis (LFA) or thermoreflectance (TR) methods, respectively.

The formular used for the calculation of the thermal conductivity λ(T) is given by [50]:

$$\lambda(T) = \rho(T)c_P(T)\mu(T) = \frac{\rho_0}{1 + 3\alpha(T)T}c_P(T)\mu(T)$$

with ρ_0 as the density at room temperature. The determination of the thermal expansion and the heat capacity can be performed using standard procedures, like the ASTM E228 and ASTM E1269 [54,55]. Because the determination of the thermal diffusivity of a small coating can be challenging, LFA and thermoreflectance as two possible methods are discussed below.

2.6.1 Laser Flash Analysis (LFA)

The flash method is used to observe a one-dimensional heat diffusion from a surface to the rear-surface of a plate-shaped specimen. The thermal diffusivity of solid materials above room temperature can be measured that way. The surface is heated through a single pulse applied using a flash lamp or laser, while the temperature change on the rear surface is recorded by an infrared pyrometer [56]. The method does not require contact with the sample, is easy to apply, reliable and the measurement times are very short. That makes the LFA method easily applicable for irradiated materials. Sample sizes are not specified by the ASTM E1461 and discs between 6mm and 30 mm in diameter and 1 to 6 mm in thickness have been successfully measured. However, LFA historically has required flat and parallel surfaces to be keep the error below 1% [57]. Recently methods have been developed to measure the thermal conductivity of tubes and rods [58,59]. Measurements before and after irradiation can be performed on pieces of the coated cladding to minimize that error. A complementary TEM and SEM analysis is recommended in such cases to verify the thicknesses of the oxide layer and Laves phase.

A range of numerical correlations are used to determine thermal diffusivity of a bulk sample via determination of the half-time measured by the pyrometer [56,60,61]. Two-layer materials, conceptually similar to and relevant to coated cladding, have been successfully investigated in the past. However, measuring the thermal conductivity of very thin layers below 0.1mm have been proven difficult [56]. Alternatives to LFA such as thermoreflectance may be useful as alternative methods to determine degradation of thermal conductivity of coated cladding following irradiation [52].

2.6.2 Thermoreflectance (TR)

The thermal diffusion time depends on the thickness and the thermal diffusivity of a sample. The thermoreflectance method has originally been developed by the National Institute of Advanced industrial Science and Technology to determine accurate thermal diffusivity of electronic devices in the nanometer range. The method uses an instrument setup as shown in Figure 13. Two lasers, a pump laser pulses periodically to irradiate the sample and a probe laser is used to detect the temperature response. It can be used in Rear Heating/ Front Detection (RF) and Front Heating / Front Detection (FF) mode for sample film thicknesses between 10 nm and 20 μm. However, even though very small thicknesses are possible to investigate accurately, the sample preparation is cumbersome. The coatings need to have a transparent (RF and FF method) or opaque substrate. In addition, a metal coating of Mo, Al, or Pt with a thickness of around 100nm should be applied on the surface as a transducer.

The above limitations of this technique in its current stage of development limit probable application to coatings on claddings. Coupon type samples, using the same processing parameters to create a similar morphology (see Figure 1), would need to be prepared and investigated to obtain the initial thermal diffusivity and thermal conductivity. In a second step, these coupons would need to undergo operation relevant temperature and irradiation treatments in a test reactor like HFIR or other beamlines to determine the change of the thermal conductivity. Even though it would be scientifically relevant to do those tests, a

series of coupons with coatings applied with different processing parameters and thicknesses would be necessary to provide a scientifically sound study. Expecting that the thermal conductivity of a thin coating of a few microns does not impact the overall thermal conductivity of the cladding significantly, it is recommended to use literature values for the thermal diffusivity and thermal conductivity of the Cr_2O_3, Cr, Laves phase, and Zr-based cladding as values for BISON simulations.

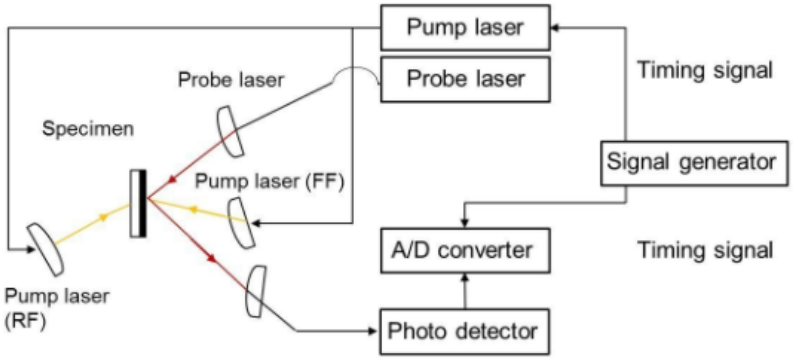

Figure 13. Instrument setup of a NanoTR apparatus *[62]*.

2.7 Irradiation Swelling

Under LWR operating conditions, it is anticipated that irradiation swelling of materials similar to the coating would be relatively insignificant: below 1% for ≈20 dpa [63]. Assuming that the coating behaves in a manner similar to BCC Fe-Cr binary alloys [63], the coating is not expected to experience significant irradiation-induced swelling. However, irradiation swelling may cause the coating to expand radially, while irradiation growth of Zircaloy typically contracts the cladding radially. This would put coating in compression in the hoop direction. Depending on the strain rate mismatch between the coating swelling and the Zircaloy cladding axial growth, this could lead to axial tension inside the coating.

The total stress of the coating can be measured using the stress measurements described in Section 2.1.1. This value accommodates the stress induced by thermal expansion and by differential irradiation swelling. The coefficient of thermal expansion (CTE) functions for the substrate and coating are known, and their contribution to the overall total stress can be calculated and modeled. The strain induced by differential irradiation swelling in the coating $\varepsilon_{C,irr}$ is given by [64,65]:

$$\varepsilon_{C,irr} = \frac{\Delta L_S - \Delta L_C}{1-\nu_C},$$

where ΔL is the fractural length change caused by irradiation, and ν_C is the Poisson ratio of the coating when the thickness of the substrate is much larger than the thickness of the coating.

In addition to calculations performed on the basis of the stress measurements using XRD, it is recommended that irradiation swelling of the coating and substrate be verified by calculating the swelling on the bases of TEM imaging techniques, as shown in Figure 14 [20]. EFTEM can be used to calculate the thickness of the TEM lamella, and the swelling can be calculated using image analysis software. The acquired data should be compared to the calculated values for coherence.

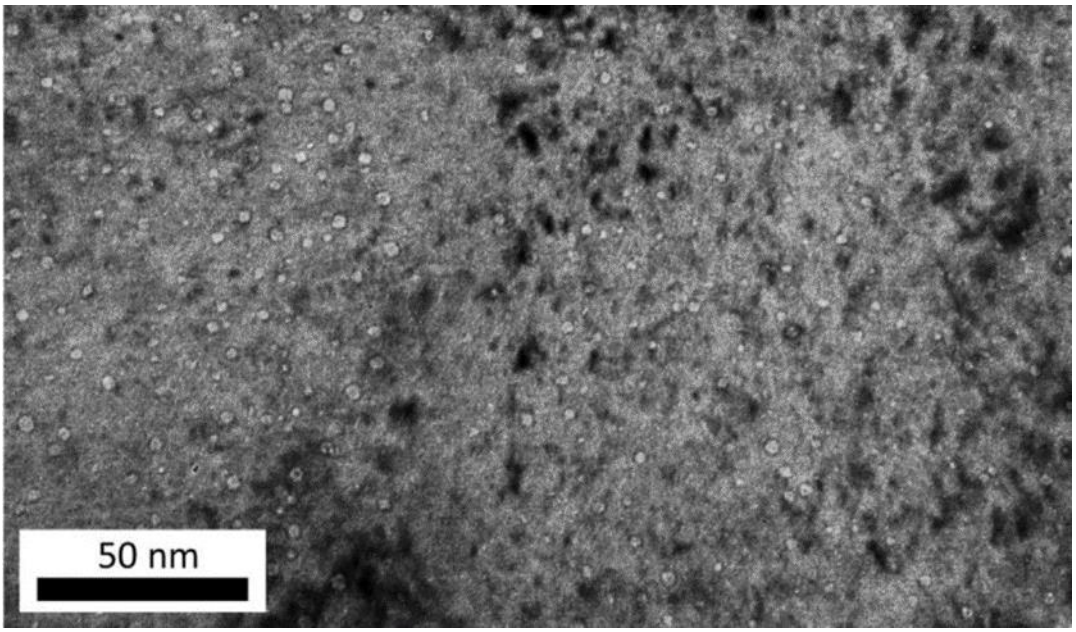

Figure 14. TEM image of Cr coating shown with an under-focus of 0.5 μm *[20]*.

2.8 Oxidation

Coating oxidation of any candidate coating material, particularly Cr-based coatings, is expected to be negligible in comparison to Zr-based alloys [10,66]. The oxidation of Zr-based alloys is a strongly exothermic reaction, which accelerates the course of accident progression, especially at high temperatures [67]. A coating is intended to prevent oxidation of the cladding material by providing an oxidation barrier. Incorporation of any coating will be exhaustively screened in this regard using established methods. This screening will be performed early in the development process given the dominate driver of accident tolerance.

However, a major question that remains is how irradiation and extended waterside corrosion during commercial nuclear reactor operation may impact the high temperature oxidation performance of coated cladding. This aspect will be critical if vendors begin seeking to take credit for performance benefits enabled by coatings. Under high-temperature conditions, the formed Cr_2O_3 will remain more passivating than Zircaloy. Even though no negative impact is expected regarding the oxidation behavior, it may be important to determine whether the oxide layer has an impact on the thermal conductivity and/or the mechanical properties of the coating. The growth of the oxide layer on Cr was found to be twentyfold less than that found on non-coated Zr-based cladding [68]. Oxidation studies have already shown the inferior oxidation properties of the Laves phase as compared to Zr, which could be detrimental if the Cr_2O_3 layer coarsens to the point that it encounters the Cr_2Zr phase [69]. The observed formation of a brittle scale composed of Zr and Cr as opposed to a protective Cr layer should be prevented.

An improved understanding of the specific oxidation rates observed during reactor service is necessary to further evaluate the role and importance of oxidation. Long-term or very high-temperature oxidation tests have been performed to confirm the calculations of the oxide growth and to investigate the impact of a growing Cr_2O_3 layer, but it is unclear how closely these observations will match those expected under the more complex oxidation environment encountered during in-core service due to radiolysis and other factors [70]. Recently, Capps et al [71] have successfully shown that the SATS in ORNL's IFEL is

capable of testing irradiated samples to various in-core conditions, including high temperatures, steam, and direct quenching [72,73]. These tests will be valuable for screening the impact of oxidation on critical performance metrics for irradiated coated cladding.

2.9 Elastic Modulus

The elastic properties of the coating may impact the cladding strain if the coating is significantly stronger than the cladding and relatively thick. In case of Cr-coated Zr-based cladding, it is expected that the E-modulus of Cr does not have a significant impact. The E-modulus of Zircaloy is nearly twice the value of Cr. However, the coating stress state has a high dependence on the E-modulus, but due to the relative thickness ratio of coating and cladding, the cladding is expected to be unaffected by the coating's elastic properties.

Verification of the elastic modulus of the coating itself, as well as any evolved secondary interphases (e.g., interface reactions and oxidation layers), can be readily obtained through nanoindentation across the interface(s), as described in Section 2.4.1. This process should be performed before and after irradiation to calculate embrittlement and to deliver data for subsequent BISON modeling. Spatial resolution of these measurements can be obtained on the sub-micrometer scale when more advanced sample mounting and characterization methods are deployed.

2.10 Specific Heat Capacity

The specific heat capacity of Cr and Cr_2O_3 are around 0.45 and 0.7 $Jg^{-1}K^{-1}$, respectively. These values are higher than the specific heat capacity of Zr (0.27 $Jg^{-1}K^{-1}$) [50,74]. As mentioned in Section 2.6, the specific heat capacity can be measured with DSC using ASTM E1269. However, this method would require bulk materials and would not be sensitive enough to detect changes induced by a thin coating of the geometry relevant to coated cladding. However, the impact of possible variations in specific heat capacity resulting from coating evolution or irradiation will be insignificant. For that reason, the specific heat capacity was evaluated to be of the lowest importance, as shown above in Table 1.

3. SUMMARY

An overview of the coating properties and the key aspects of cladding performance that are anticipated to be impacted by coatings is provided, as well as a ranking, to highlight the most pressing concerns and research areas necessary to improve understanding of coated cladding. Residual stress, creep, and the kinetics / outcomes of eutectic formation were identified as research areas in which further work is necessary to gather information about the coating-cladding relationship under reactor conditions.

Neither residual stress determination nor creep measurement has well-established test methods applicable to coated nuclear reactor cladding. Residual stress measurement of coated tube geometries has been demonstrated in other fields, but application and optimization of these methods to the relevant geometries is needed. Creep in coated cladding is a complex phenomenon that involves the confluence of temperature, irradiation, and possible compositional effects. Methods exist that can measure creep after test reactor irradiations, but to date, these methods have only been demonstrated for a small number of conditions. Further work is warranted to understand this important behavior, with particular emphasis on development of testing methods that can serve as predictions of irradiation creep without requiring integral testing. Finally, the kinetics of eutectic formation in unirradiated material at relevant temperatures does not pose any technique challenges, but test irradiations will be required to improve understanding of irradiation enhancement to this behavior.

4. REFERENCES

[1] K.A. Terrani, *Report on Design and Failure Limits of SiC/SiC and FeCrAl ATF Cladding Concepts under RIA*. ORNL/LTR-2018/521, Oak Ridge National Laboratory, Approved for Public Release (2018).

[2] C. Tang, M. Stueber, H.J. Seifert, M. Steinbrueck, "Protective Coatings on Zirconium-Based Alloys as Accident-Tolerant Fuel (ATF) Claddings," *Corros. Rev.* 35 (2017) 141–165. https://doi.org/10.1515/corrrev-2017-0010.

[3] M. Kurata, "Research and Development Methodology for Practical Use of Accident Tolerant Fuel in Light Water Reactors," *Nucl. Eng. Technol.* 48 (2016) 26–32. https://doi.org/10.1016/j.net.2015.12.004.

[4] P. Hosemann, "Small-Scale Mechanical Testing on Nuclear Materials: Bridging the Experimental Length-Scale Gap," *Scr. Mater.* 143 (2018) 161–168. https://doi.org/10.1016/j.scriptamat.2017.04.026.

[5] T. Shinozaki, Y. Udagawa, T. Mihara, T. Sugiyama, M. Amaya, "Improved-EDC Tests on the Zircaloy-4 Cladding Tube with an Outer Surface Pre-Crack," J. *Nucl. Sci. Technol.* 53 (2016) 1426–1434. https://doi.org/10.1080/00223131.2015.1123658.

[6] T. Jezequel, Q. Auzoux, D. Le Boulch, M. Bono, E. Andrieu, C. Blanc, V. Chabretou, N. Mozzani, M. Rautenberg, "Stress Corrosion Crack Initiation of Zircaloy-4 Cladding Tubes in an Iodine Vapor Environment during Creep, Relaxation, and Constant Strain Rate Tests," *J. Nucl. Mater.* 499 (2018) 641–651. https://doi.org/10.1016/j.jnucmat.2017.07.014.

[7] H. Li, T. Koyanagi, X. Hu, Y. Katoh, "Multiscale Experimental Characterization of Coatings on Ceramics: A Case Study of Tungsten on SiC," *Surf. Coatings Technol.* 367 (2019) 1–10. https://doi.org/10.1016/j.surfcoat.2019.03.040.

[8] J. Chen, S.J. Bull, "Approaches to Investigate Delamination and Interfacial Toughness in Coated Systems: An Overview," *J. Phys. D. Appl. Phys.* 44 (2011). https://doi.org/10.1088/0022-3727/44/3/034001.

[9] H. Chen, X. Wang, R. Zhang, "Application and Development Progress of Cr-Based Surface Coating in Nuclear Fuel Elements: II. Current Status and Shortcomings of Performance Studies," *Coatings*. 10 (2020). https://doi.org/10.3390/coatings10090835.

[10] M. Wagih, B. Spencer, J. Hales, K. Shirvan, "Fuel Performance of Chromium-Coated Zirconium Alloy and Silicon Carbide Accident Tolerant Fuel Claddings," *Ann. Nucl. Energy.* 120 (2018) 304–318. https://doi.org/10.1016/j.anucene.2018.06.001.

[11] A.-M. Velente-Feliciano, Hipims, "A New Generation of Film Deposition Techniques for SRF Applications," *Proc. SRF2013*. (2013) 754–760.

[12] J.C. Brachet, I. Idarraga-Trujillo, M. Le Flem, M. Le Saux, V. Vandenberghe, S. Urvoy, E. Rouesne, T. Guilbert, C. Toffolon-Masclet, M. Tupin, C. Phalippou, F. Lomello, F. Schuster, A. Billard, G. Velisa, C. Ducros, F. Sanchette, "Early Studies on Cr-Coated Zircaloy-4 as Enhanced Accident Tolerant Nuclear Fuel Claddings for Light Water Reactors," *J. Nucl. Mater.* 517 (2019) 268–285. https://doi.org/10.1016/j.jnucmat.2019.02.018.

[13] J. Ribis, A. Wu, J. Brachet, E. Clouet, B. Arnal, E. Rouesne, S. Urvoy, F. Barcelo, A. Gentils, C. Baumier, L. Rancoeur, Y. Robert, F. Leprêtre, J. Bischoff, E. Pouillier, "Chromium Hardening and Zr-Cr Interface Stability of Irradiated Chromium-Coated Zircaloy-4 Alloy" (2018). https://hal-cea.archives-ouvertes.fr/cea-02400192 (accessed December 31, 2020).

[14] ATI Metals, *Zircaloy-4 Annealed - Technical Data Sheet*, 1 (2015) 2014–2016.

https://www.atimetals.com/Products/Documents/datasheets/zirconium/alloy/Zr_nuke_waste_disposal_v2.pdf.

[15] N.A. Dubrovinskaia, L.S. Dubrovinsky, S.K. Saxena, B. Sundman, "Thermal Expansion of Chromium (Cr) to Melting Temperature," *Calphad* Comput. Coupling Phase Diagrams Thermochem. 21 (1997) 497–508. https://doi.org/10.1016/S0364-5916(98)00007-8.

[16] K. Geelhood, W. Luscher, *Degradation and Failure Phenomena of Accident Tolerant Fuel Concepts - Chromium Coated Zirconium Alloy Cladding*, PNNL-28437 (2019).

[17] T. Ohta, Y. Nakagawa, Y. Kaneno, H. Inoue, T. Takasugi, W.Y. Kim, "Microstructures and Mechanical Properties of NbCr2 and ZrCr2 Laves alloys Prepared by Powder Metallurgy," *J. Mater. Sci.* 38 (2003) 657–665. https://doi.org/10.1023/A:1021807519728.

[18] J. Ribis, A. Wu, J.C. Brachet, F. Barcelo, B. Arnal, "Atomic-Scale Interface Structure of a Cr-Coated Zircaloy-4 Material," *J. Mater. Sci.* 53 (2018) 9879–9895. https://doi.org/10.1007/s10853-018-2333-1.

[19] I. V. Oryshich, N.E. Poryadchenko, N.P. Brodnikovskii, "High-Temperature Oxidation of Intermetallics Formed by Group IV Transition Metals with Chromium," *Powder Metall. Met. Ceram.* 43 (2004) 497–503. https://doi.org/10.1007/s11106-004-0011-0.

[20] P.J. Doyle, T. Koyanagi, C. Ang, L. Snead, P. Mouche, Y. Katoh, S.S. Raiman, "Evaluation of the Effects of Neutron Irradiation on First-Generation Corrosion Mitigation Coatings on SiC for Accident-Tolerant Fuel Cladding," *J. Nucl. Mater.* 536 (2020) 152203. https://doi.org/10.1016/j.jnucmat.2020.152203.

[21] K. Knipe, A. Manero, S.F. Siddiqui, C. Meid, J. Wischek, J. Okasinski, J. Almer, A.M. Karlsson, M. Bartsch, S. Raghavan, "Strain Response of Thermal Barrier Coatings Captured under Extreme Engine Environments through Synchrotron X-Ray Diffraction," *Nat. Commun.* 5 (2014) 1–7. https://doi.org/10.1038/ncomms5559.

[22] P.S. Prevey, "X-Ray Diffraction Residual Stress Techniques," in: *Mater. Charact., ASM International*, 1986: pp. 380–392. https://doi.org/10.31399/asm.hb.v10.a0001761.

[23] G.S. Schajer, *Practical Residual Stress Measurement Methods*, 2013. https://doi.org/10.1002/9781118402832.

[24] N. Norberg, A.C. Vermeulen, "Effects of Misalignment of Parallel Beam Optics on Thin Film Stress Analysis," *Adv. Mater. Res.* 996 (2014) 141–146. https://doi.org/10.4028/www.scientific.net/AMR.996.141.

[25] J. Malzbender, J.M.J. Den Toonder, A.R. Balkenende, G. De With, "Measuring Mechanical Properties of Coatings: A Methodology Applied to Nano-Particle-Filled Sol-Gel Coatings on Glass, *Mater. Sci. Eng. R Reports*. 36 (2002) 47–103. https://doi.org/10.1016/s0927-796x(01)00040-7.

[26] L.E. Koutsokeras, G. Abadias, "Intrinsic Stress in ZrN Thin Films: Evaluation of Grain Boundary Contribution from In Situ Wafer Curvature and Ex Situ X-Ray Diffraction Techniques," *J. Appl. Phys.* 111 (2012). https://doi.org/10.1063/1.4710530.

[27] J. Dean, G. Aldrich-Smith, T.W. Clyne, "Use of Nanoindentation to Measure Residual Stresses in Surface Layers," *Acta Mater.* 59 (2011) 2749–2761. https://doi.org/10.1016/j.actamat.2011.01.014.

[28] H. Okamoto, "Supplemental Literature Review of Binary Phase Diagrams: B-Fe, Cr-Zr, Fe-Np, Fe-W, Fe-Zn, Ge-Ni, La-Sn, La-Ti, La-Zr, Li-Sn, Mn-S, and Nb-Re," *J. Phase Equilibria Diffus.*

37 (2016) 621–634. https://doi.org/10.1007/s11669-016-0465-z.

[29] M.N. Cinbiz, B. Garrison, R.R. Lowden, R.G. Sitterson, K. Linton, *Progress Report on Modified Burst Testing and Alternative Test Methodologies*, ORNL/SPR-2019/1129 (2019). https://www.osti.gov/servlets/purl/1530086.

[30] J. Brachet, M. Dumerval, M. Le Saux, E. Rouesne, S. Urvoy, T. Guilbert, Q. Houmaire, C. Cobac, "Behavior of Chromium Coated M5TM Claddings under LOCA Conditions," *WRFPM 2017 Water React. Fuel Perform. Meet.* (2017).

[31] R.B. Rebak, M. Larsen, Y.-J. Kim, "Characterization of Oxides Formed on Iron-Chromium-Aluminum Alloy in Simulated Light Water Reactor Environments," *Corros. Rev.* 35 (2017) 177–188. https://doi.org/10.1515/corrrev-2017-0011.

[32] H.J. Lu, W.B. Wang, N. Zou, J.Y. Shen, X.G. Lu, Y.L. He, "Thermodynamic Modeling of Cr-Nb and Zr-Cr with Extension to the Ternary Zr-Nb-Cr System," *Calphad Comput. Coupling Phase Diagrams Thermochem.* 50 (2015) 134–143. https://doi.org/10.1016/j.calphad.2015.06.002.

[33] Y. Matsuo, "Thermal Creep of Zircaloy-4 Cladding under Internal Pressure," *J. Nucl. Sci. Technol.* 24 (1987) 111–119. https://doi.org/10.1080/18811248.1987.9735783.

[34] D.O. Hobson, *Creepdown of Zircaloy Fuel Cladding: Initial Tests [BWR; PWR]*, ORNL/NUREG/TM-181, Oak Ridge, Tennessee, 1978. https://doi.org/10.2172/5011430.

[35] J.R. Stephens, W.D. Klopp, "High-Temperature Creep of Polycrystalline Chromium," *J. Less-Common Met.* 27 (1972) 87–94. https://doi.org/10.1016/0022-5088(72)90108-7.

[36] M. Limbäck, T. Andersson, "A Model for Analysis of the Effect of Final Annealing on the In-and Out-of-Reactor Creep Behavior of Zircaloy Cladding," ASTM Spec. Tech. Publ. 1295 (1996) 448–468. https://doi.org/10.1520/stp16185s.

[37] F.A. Garner, M.B. Toloczko, B.H. Sencer, "Comparison of Swelling and Irradiation Creep Behavior of fcc-Austenitic and bcc-Ferritic/Martensitic Alloys at High Neutron Exposure," *J. Nucl. Mater.* 276 (2000) 123–142. https://doi.org/10.1016/S0022-3115(99)00225-1.

[38] P.L. Mulligan, H. Sakasegawa, H. Tanigawa, C.M. Petrie, J.L. McDuffee, Y. Katoh, "An F82H Steel Pressurized Tube Creep Capsule for Irradiation in HFIR," *Nucl. Mater. Energy.* 15 (2018) 254–260. https://doi.org/10.1016/j.nme.2018.05.011.

[39] P. Mulligan, S. Clark, A. Nelson, Pre-Irradiation Characterization of ARMOR Coated Zircaloy Pressurized Creep Tubes, ORNL/SPR-2020/1538, May 2020.

[40] R.S. Gordon, *Thin Films and Coatings*, Wiley Online Library, 2007. https://doi.org/10.1002/9780470145333.ch148.

[41] J. Chen, L. Lu, K. Lu, "Hardness and Strain Rate Sensitivity of Nanocrystalline Cu," *Scr. Mater.* 54 (2006) 1913–1918. https://doi.org/10.1016/j.scriptamat.2006.02.022.

[42] K. Durst, V. Maier, "Dynamic Nanoindentation Testing for Studying Thermally Activated Processes from Single to Nanocrystalline Metals," *Curr. Opin. Solid State Mater. Sci.* 19 (2015) 340–353. https://doi.org/10.1016/j.cossms.2015.02.001.

[43] H. Takagi, M. Fujiwara, "Set of Conversion Coefficients for Extracting Uniaxial Creep Data from Pseudo-Steady Indentation Creep Test Results," *Mater. Sci. Eng. A.* 602 (2014) 98–104. https://doi.org/10.1016/j.msea.2014.02.060.

[44] D.A. Lucca, K. Herrmann, M.J. Klopfstein, "Nanoindentation: Measuring Methods and Applications," *CIRP Ann. - Manuf. Technol.* 59 (2010) 803–819. https://doi.org/10.1016/j.cirp.2010.05.009.

[45] P. Mouche, T. Koyanagi, D. Patel, Y. Katoh, "Adhesion, Structure, and Mechanical Properties of Cr HiPIMS and Cathodic Arc Deposited Coatings on SiC," *Surf. Coatings Technol.* (Under Rev. (n.d.).

[46] D. Chicot, P. Démarécaux, J. Lesage, Apparent Interface Toughness of Substrate and Coating Couples from Indentation Tests," *Thin Solid Films.* 283 (1996) 151–157. https://doi.org/10.1016/0040-6090(96)08763-9.

[47] H.G. Kim, I.H. Kim, Y. Il Jung, D.J. Park, J.Y. Park, Y.H. Koo, "Adhesion Property and High-Temperature Oxidation Behavior of Cr-Coated Zircaloy-4 Cladding Tube Prepared by 3D Laser Coating, *J. Nucl. Mater.* 465 (2015) 531–539. https://doi.org/10.1016/j.jnucmat.2015.06.030.

[48] "Supplemental Guidance Regarding the Chromium-Coated Zirconium Alloy Fuel Cladding Accident Tolerant Fuel Concept Interim Staff Guidance," NRC Notice (2020).

[49] S. Pathak, S.R. Kalidindi, "Spherical Nanoindentation Stress-Strain Curves," *Mater. Sci. Eng. R Reports.* 91 (2015) 1–36. https://doi.org/10.1016/j.mser.2015.02.001.

[50] U. Holzwarth, H. Stamm, "Mechanical and Thermomechanical Properties of Commercially Pure Chromium and Chromium Alloys," *J. Nucl. Mater.* 300 (2002) 161–177. https://doi.org/10.1016/S0022-3115(01)00745-0.

[51] J.B. Ainscough, "Gap Conductance in Zircaloy-Clad LWR Fuel Rods," United Kingdom At. Energy Auth. (1982).

[52] R. Cheaito, C.S. Gorham, A. Misra, K. Hattar, P.E. Hopkins, "Thermal Conductivity Measurements via Time-Domain Thermoreflectance for the Characterization of Radiation Induced Damage," *J. Mater. Res.* 30 (2015) 1403–1412. https://doi.org/10.1557/jmr.2015.11.

[53] F. Stein, A. Leineweber, "Laves Phases: a Review of Their Functional and Structural Applications and an Improved Fundamental Understanding of Stability and Properties," *J. Mater. Sci.* 56 (2021) 5321–5427. https://doi.org/10.1007/s10853-020-05509-2.

[54] *Standard Test Method for Determining Specific Heat Capacity by Differential Scanning Calorimetry*, American Society for Testing and Materials, E1269-0114 (2001) E 1269-01. https://doi.org/10.1520/E1269-11R18.

[55] *Standard Test Method for Linear Thermal Expansion of Solid Materials with a Vitreous Silica Dilatometer*, ASTM E228-17, ASTM Int. (n.d.). https://doi.org/10.1520/E0228-17.

[56] M. Akoshima, T. Tanaka, S. Endo, Tetsuya Baba, Y. Harada, Y. Kojima, A. Kawasaki, F. Ono, "Thermal Diffusivity Measurement for Thermal Spray Coating Attached to Substrate Using Laser Flash Method," *Jpn. J. Appl. Phys.* 50 (2011). https://doi.org/10.1143/JJAP.50.11RE01.

[57] Standard Test Method for Thermal Diffusivity by the Flash Method, ASTM E1461-13, ASTM Int. (2013). https://doi.org/10.1520/E1461-13.

[58] A. Salazar, F. Garrido, R. Celorrio, "Thermal Diffusivity of Rods, Tubes, and Spheres by the Flash Method," *J. Appl. Phys.* 99 (2006) 066116. https://doi.org/10.1063/1.2183584.

[59] L. Fave, M.A. Pouchon, C. Hébert, "A Radial Heat Flow Apparatus for Thermal Conductivity Characterisation of Cylindrical Samples," *J. Therm. Anal. Calorim.* 130 (2017) 1855–1863. https://doi.org/10.1007/s10973-017-6578-8.

[60] C.P.B. and G.L.A. W. J. Parker, R. J. Jenkins, "Flash Method of Determining Thermal Diffusivity," *J. Appl. Phys.*, Springer Netherlands, Dordrecht, 1961: pp. 1679–1684. https://doi.org/10.1007/978-94-007-2739-7_100240.

[61] E.J. Carr, "Rear-Surface Integral Method for Calculating Thermal Diffusivity from Laser Flash Experiments," *Chem. Eng. Sci.* 199 (2019) 546–551. https://doi.org/10.1016/j.ces.2019.01.014.

[62] NETSCH, https://www.netzsch-thermal-analysis.com/us/products-solutions/thermal-diffusivity-conductivity/nanotrpicotr/.

[63] R.L. Klueh, "Elevated Temperature Ferritic and Martensitic Steels and Their Application to Future Nuclear Reactors," *Int. Mater. Rev.* 50 (2005) 287–310. https://doi.org/10.1179/174328005X41140.

[64] V. Teixeira, "Residual Stress and Cracking in Thin PVD Coatings," *Vacuum* 64 (2002) 393–399.

[65] V. Teixeira, "Mechanical Integrity in PVD Coatings Due to the Presence of Residual Stresses," *Thin Solid Films.* 392 (2001) 276–281. https://doi.org/10.1016/S0040-6090(01)01043-4.

[66] J.C. Brachet, T. Guilbert, M. Le Saux, J. Rousselot, G. Nony, C. Toffolon-Masclet, A. Michau, F. Schuster, H. Palancher, J. Bischoff, J. Augereau, E. Pouillier, "Behavior of Cr-Coated M5 Cladding during and after High Temperature Steam Oxidation from 800°C up to 1500°C (LOCA & Design Extension Conditions), *TopFuel 2018*. (2018) A0100.

[67] *Accident Tolerant Fuel Concepts for Light Water Reactors*, Proc. International Atomic Energy Agency Technical Meeting (2014).

[68] H.G. Kim, I.H. Kim, Y. Il Jung, D.J. Park, J.H. Yang, Y.H. Koo, "Development of Surface Modified Zr Cladding by Coating Technology for ATF," *Top Fuel 2016 LWR Fuels with Enhanc. Saf. Perform.* (2016) 1157–1163.

[69] M.K. Ferber, A.A. Wereszczak, M. Lance, J.A. Haynes, M.A. Antelo, "Application of Infrared Imaging to the Study of Controlled Failure of Thermal Barrier Coatings," *J. Mater. Sci.* 35 (2000) 2643–2651. https://doi.org/10.1023/A:1004781220825.

[70] J.-C. Brachet, T. Guilbert, M. Le Saux, F. Lomello, "Behavior of Cr Coated M5 Claddings under LOCA Conditions," *Water React. Fuel Perform. Meet.* (2017).

[71] N. Capps, Y. Yan, A. Raftery, Z. Burns, T. Smith, K. Terrani, K. Yueh, M. Bales, K. Linton, "Integral LOCA Fragmentation Test on High-Burnup Fuel," *Nucl. Eng. Des.* 367 (2020) 110811. https://doi.org/10.1016/j.nucengdes.2020.110811.

[72] K.D. Linton, Z.M. Burns, K.A. Terrani, Y. Yan, *Hot Cell Installation and Demonstration of the Severe Accident Test Station*, ORNL/SPR-2017/434, Oak Ridge National Laboratory (2017). https://www.osti.gov/servlets/purl/1394377.

[73] M. Snead, Y. Yan, M. Howell, J. Keiser, K. Terrani, *Severe Accident Test Station Design Document*, ORNL/TM-2015/556, Oak Ridge National Laboratory, 2015.

[74] *NIST Chemistry Webbook* (2021.). https://webbook.nist.gov/cgi/inchi?ID=C7440473&Type=JANAFS&Table=on#JANAFS.